Classification of quantum states of light using random measurements through a multimode fiber

Saroch Leedumrongwatthanakun,[1,2,3,*] Luca Innocenti,[4,5] Alessandro Ferraro,[5,6] Mauro Paternostro,[4,5] and Sylvain Gigan[1]

[1]*Laboratoire Kastler Brossel, ENS-PSL Research University, CNRS, Sorbonne Université, Collège de France, 24 rue Lhomond, 75005 Paris, France*

[2]*Institute of Photonics and Quantum Sciences, Heriot-Watt University, Edinburgh EH14 4AS, United Kingdom*

[3]*Division of Physical Science, Faculty of Science, Prince of Songkla University, Hat Yai, Songkhla 90110, Thailand*

[4]*Università degli Studi di Palermo, Dipartimento di Fisica e Chimica – Emilio Segrè, via Archirafi 36, I-90123 Palermo, Italy*

[5]*Centre for Quantum Materials and Technologies, School of Mathematics and Physics, Queen's University Belfast, Belfast BT7 1NN, United Kingdom*

[6]*Dipartimento di Fisica "Aldo Pontremoli," Università degli Studi di Milano, I-20133 Milano, Italy*

(Received 9 December 2023; accepted 12 February 2025; published 3 June 2025)

Extracting meaningful information about unknown quantum states without performing a full tomography is an important task. Low-dimensional projections and random measurements can provide such insight but typically require careful crafting. In this paper, we present an optical scheme based on sending unknown input states through a multimode fiber and performing two-point intensity and coincidence measurements. A short multimode fiber implements effectively a random projection in the spatial domain, while a long-dispersive multimode fiber performs a spatial and spectral projection. We experimentally show that useful properties, i.e., the purity, dimensionality, and degree of indistinguishability of various states of light including spectrally entangled biphoton states, can be obtained by measuring statistical properties of single counts and their correlation between two outputs over many realizations of unknown random projections. Moreover, we show that this information can then be used for state classification.

DOI: 10.1103/PhysRevResearch.7.023222

I. INTRODUCTION

The evolution of a system of interest through an uncharacterized quantum channel transforms the state in an undesirable and seemingly detrimental way. Examples include unknown rotation of polarization through optical fibers, optical aberrations induced by atmospheric turbulence, and fluctuations of magnetic and electric fields in systems of trapped ions and cold atoms. Random matrix theory (RMT), which was originally developed to understand distributions of energy level spacings of heavy nuclei [1], can be used to successfully describe the statistical features arising from random evolutions. The breadth of its applications covers many areas of physics [2–4], all the way to information processing, where RMT has been insightfully applied to address compressed sensing [5], random features of large-scale kernel machines [6], and randomized algorithms for very large matrices [7]. In quantum physics, randomized measurements —a method of extracting information about the system of interest by performing measurements in random bases drawn from a certain ensemble — have benefited from the use of RMT. Such an approach has been applied for the detection of entanglement in many-body systems without sharing reference frames between parties [8–15], the verification of quantum devices [16–19], and the simplification of state tomography [20–26], among other tasks, thus consolidating its usefulness in estimating state properties with only a few copies [27–31]. This is not only remarkable but also a very valuable tool for the grounding of approaches to the characterization of quantum states and processes that do not rely on fully tomographic methods [32,33]. The latter being typically very resource expensive, set a *de facto* severe constraint to the scaling up of quantum technologies and their validation.

In optics, the propagation of light through scattering media or random interferometric processes is well described via RMT [34,35], and results in complicated intensity patterns, known as speckles [36]. They can be observed in interferograms of high-order intensity correlations, referred to as *coincidence speckle*, and embody an interesting effect of optical coherence [37,38] that stems from the interplay of interference, indistinguishability, and correlations. Over the last two decades, substantial endeavours have been devoted to understanding the evolution of nonclassical lights in complex scattering processes [34,39]. A wide range of topics has been theoretically investigated, for instance, the degradation of entanglement due to truncated and multimode detections [40–44], the transport of quantum noise [45–49], and the dynamics of photon statistics in disordered or structured medium [50–53]. However, only a modest number of experiments have been carried out in this area [42,54–58]. In particular, one of

*Contact author: saroch.l@psu.ac.th

Published by the American Physical Society under the terms of the Creative Commons Attribution 4.0 International license. Further distribution of this work must maintain attribution to the author(s) and the published article's title, journal citation, and DOI.

the intriguing predictions in this field is the presence of spatial intensity correlation averaged over many settings of random unknown measurements [54,55,59,60]. The spatial intensity correlations in twofold coincidence speckles result from both classical and quantum origins [61–63] and depends upon both the scattering properties of a medium and the state of the incident light [54,55,60,62,64–67].

For a spatially maximally entangled biphoton state, the statistical distribution of twofold coincidence speckles has been applied to predict purity and entanglement dimensionality [68]. An experimental demonstration based on the use of rotating diffusers as reprogrammable random transformations has been reported in Ref. [58]. In the context of the boson sampling problem, the statistical moments of two-point spatial correlations have been recently used to certify the degree of indistinguishability of many-particle quantum interference [65,67,69]. This has been experimentally applied to classify the indistinguishability of three-photon interference on seven-mode integrated photonic waveguides [70]. The statistical distribution of two-point spatial correlation [67] has been used to validate the quantum interference of 50 indistinguishable single-mode squeezed states on a 100-mode phase-stabilized interferometer by ruling out the plausible hypotheses of outcome stemming from thermal states and distinguishable photons [71]. These works pave the way for the use of random, unknown measurements to estimate and classify quantum states. However, a handy optical device that can be implemented across different degrees of freedom of light, the extension of theoretical studies over various classes of states, and the limitations of the techniques when noises such as dark counts and accidental coincidences are presented, are still lacking.

In this work, we tackle these problems and propose a simple optical implementation of a reconfigurable random transformation obtained by randomly sending a state of light through a multimode fiber using a spatial light modulator. By changing the length of the fiber to increase dispersions, this implementation allows exploiting, besides the polarization and spatial degrees of freedom, also the temporal modes of light. We employ the proposed apparatus to demonstrate the use of random photon-counting measurements, second-order intensity correlations (twofold coincidences), and normalized second-order intensity correlation between two truncated output modes, to probe the properties of input states for the purposes of state classification. Various paradigmatic input states, such as one- and two-photon states, N00N states, and spectrally entangled biphoton states are used in our experimental demonstration.

We observe the flattening of the statistical distribution of normalized second-order intensity correlation due to the presence of two-photon interference, which indicates a good measure of the degree of indistinguishability as compared to that computing from the unnormalized two-fold coincidences widely used in previous seminal demonstrations. The study of statistics of normalized and unnormalized second-order intensity correlation is also extended to the presence of spectral-temporal entanglement and dispersions. We demonstrate that the use of random measurements on the three types of detected signals reveals useful distinct statistical signatures. By jointly analyzing statistical moments of these outcomes, we resolve the properties of the input states, including the purity, dimensionality, and indistinguishability, which are then used to classify the states without the need to perform full state tomography. The simplicity of the setting put forward in this implementation as well as our study on the accuracy in characterizing the state properties shows the potential of the proposed experiment to embody a valuable tool in the quest for a resource-effective classification of quantum states of light.

II. IMPLEMENTATION OF RANDOM MEASUREMENT

We implement random transformations by evolving input states through a spatial light modulator (SLM) and a graded-index multimode fiber (MMF), acting jointly as a random interferometer (Fig. 1). In detail, light from two polarization-maintaining single mode fibers in horizontal polarization is coupled into the input ports of the interferometer. Each input port is expanded to have a beam diameter of 6.0 mm and projected onto the SLM screen (Hamamatsu, X10468-02) that is split into two parts for each input referred to as SLM_1 and SLM_2. On each input, we display a random phase pattern, constructed from the superposition of gratings with random orientations and periods to randomly excite different spatial modes of the MMF (the core diameter of 50-μm and the numerical aperture of 0.20). 25 random gratings are drawn from the ensemble of corresponding diffraction-limited spots on the isometric grid defined over the input facet of the fiber. Light from two input ports is combined using the half-wave plate (HWP) and the polarizing beamplitter (PBS) to be a co-propagating beam on two orthogonal polarizations (horizontal (H) and vertical (V) polarization). Light from two inputs is then coupled through the MMF by using the *2f*-lens system with the effective focal length of 15 mm. The *2f*-lens system consists of 200-mm, 100-mm plano-convex lenses, and 7.5-mm aspheric lens placed on the fiber alignment stages. The length of the MMF can be selected to adjust the degree of modal dispersion occurring through the MMF.

Many random transformations can be realized by displaying different phase patterns on the SLMs, which controls light coupling through the MMF propagating onto the large output space defined over polarization, spatiotemporal degrees of freedom. We here consider the scenario where an input state from the two single-mode fibers evolves through the random interferometer, and therefore the dimension of the input state is smaller than the total number of propagating (polarization-spatial) modes of the MMF at a given frequency. Moreover, we study the case where the random measurement is performed only on two fixed output modes, thus establishing our approach as being of a constrained-resource nature. Since the random interferometer is sufficiently large, unitary, and random, the random transformation on two truncated output spaces can be considered to be efficiently drawn from an independent and identically distributed complex Gaussian random matrix [72]. This means that correlations and unitary constraint presented in a subpart transmission matrix of the MMF linking to two truncated outputs is negligible, provided that the number of truncated modes ($p = 2$) satisfies $p \leqslant m^{1/6}$ [73] with $m \sim 400$ the number of modes propagating across the optical fiber. The statistical property of the random

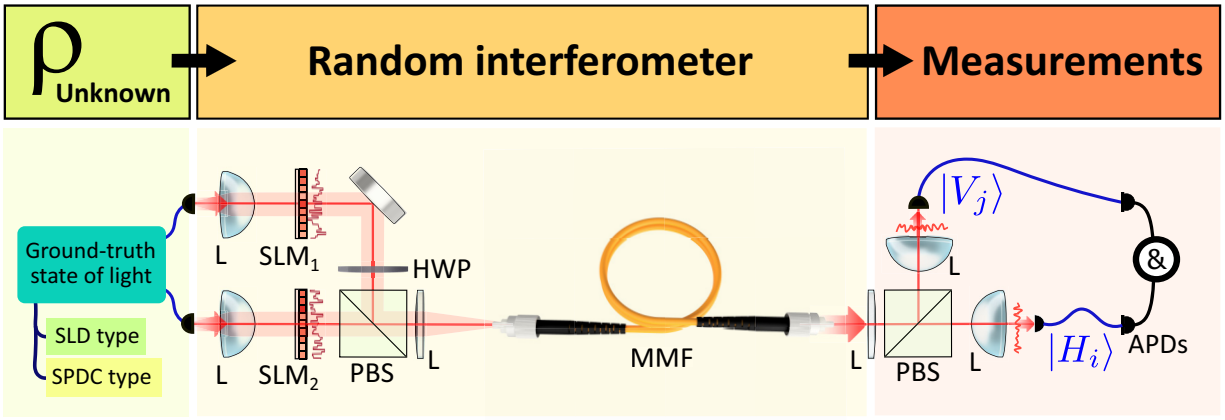

FIG. 1. Concept and experimental scheme: An unknown state of light ρ_{unknown} is evolved through a random interferometer and mapped onto a high-dimensional output that is subjected to a measurement step. The statistical features of the outcomes are used to infer properties of the state. In the experiment, ground-truth states of light, as listed in Sec. III, have been generated through spontaneous parametric down-conversion (SPDC) and superluminescent diode (SLD). Such states are randomly launched into a multimode fiber (MMF) using the spatial light modulators SLM_1 and SLM_2 that are placed on the Fourier plane of two input orthogonal polarization channels of the MMF. At each setting of random measurement, randomly generated holograms are displayed on the SLMs, and a state is controlled and evolves through the MMF. We probed the output states on randomly selected two-mode subspaces assigned at two different diffraction-limited spots on the near-field plane of the MMF and associated with orthogonal polarizations, labeled $|H_i\rangle$ and $|V_j\rangle$. Single counts (I), two-fold coincidence counts (C), and normalized second-order intensity correlation ($g^{(2)}$) are measured by avalanche photodiodes and a coincidence electronic circuit with the coincidence window of 2.5 ns. (L: lenses, HWP: half-wave plate, PBS: polarizing beamsplitter).

transformation onto two truncated outputs is provided in the Supplemental Material S.3 [74] accompanying the article.

For a given measurement setting, single counts at two outputs I_1 and I_2, and twofold coincidence counts C are measured by threshold non-resolved photon-number detectors implemented by avalanche photodiodes (SPCM-AQ4C, Excelitas) within a coincidence window τ_C. The normalized second-order intensity correlation $g^{(2)}$ is determined as $g^{(2)} = C/R$, where we have introduced the accidental coincidences $R = \tau_C I_1 I_2$. The details of the experimental setting are provided in Supplemental Material S.2 and S.4 [74].

III. GROUND-TRUTH STATES

We test the ability of our apparatus to perform state classification with a set of states spanning one and two spatial modes. The first state we consider is a mixture of two spatial modes generated by the amplified spontaneous emission of a superluminescent diode (SLD) passing through a bandpass filter. The central wavelength and the full width at half maximum of the incoherent source are $\lambda \pm \Delta\lambda = 810 \pm 2.35$ nm. Such incoherent radiation is used as a benchmark classical state to validate our approach. The remaining ground-truth states are then prepared from type-II spontaneous parametric down-conversion (SPDC) by pumping a 9.1-mm-long periodically poled potassium titanyl phosphate crystal (ppKTP) with a 405-nm continuous-wave laser at 40 mW (DLproHP, Toptica). The biphoton states are prepared in the single spatial mode generation, i.e., the pump beam is focused on the crystal such that the joint-transverse momentum amplitude of the SPDC source is almost separable and thus efficiently coupled into the two polarization-maintaining single-mode fibers [75,76]. We prepare the photon pairs in the same horizontal polarization readily to send to the random interferometer. The correspondingly generated spatially separable biphoton states are entangled in frequency and the marginal spectra of single-photon states are $\lambda \pm \Delta\lambda = 810 \pm 1.56$ nm (See the Supplemental Material [74] for the joint spectral amplitude of the SPDC source). The degree of indistinguishability of the ground-truth biphoton states is controlled by adjusting the temporal delay δ between signal and idler photons. A two-photon Fock state and an $N = 2$ N00N state $(|2_H 0\rangle + |02_V\rangle)/\sqrt{2}$, where the subscript H and V refer to the input port of the random interferometer, are generated using Hong-Ou-Mandel (HOM) interferences through fused fiber optic coupler [77,78]. The HOM visibilities of the sources before and after the experiment are provided in the Supplemental Material S.4 [74]. Finally, a heralded single-photon source is generated through a heralded approach [79].

By varying the lengths of the MMF, we can spatially control the temporal mixing of the interferometer, therefore being able to produce both narrowband and broadband states. For the bandwidth of our sources, a length of 55 cm and 25 m correspond to narrowband (non-dispersive) and broadband (dispersive) regimes, respectively. In the narrowband regime, all states were tested. In the broadband regime, where random different spatial modes are allowed to be mapped to the temporal domain owing to the modal dispersion, only SLD source, indistinguishable, and distinguishable biphoton states, were studied. Our experimental characterization has also shown that the HOM visibility of the sources is preserved after propagating through the 55-cm long MMF, and persists when using the 25-m long fiber.

IV. RESULTS AND DISCUSSIONS

Statistical moments and distributions of outcomes from random measurements can be used to infer various properties

of the unknown states. Building on the theoretical framework presented in Supplemental Material S.1 [74], here we demonstrate the use of statistical markers to achieve quantum state classification. In particular, in Sec. IV A, we demonstrate recovery of the number of occupied modes, purity, and entanglement dimensionality for input maximally entangled two-photon states. We then report the effect of quantum interference on the normalized second-order correlation function and propose a figure of merit for measuring the degree of indistinguishability based on its first two statistical moments in Sec. IV B. The figure of merit that is the visibility of the normalized second-order correlation is then studied in the presence of dispersion and frequency entanglement as discussed in Sec. IV C. Finally, an example of state classification based on such properties is given in Sec. IV D.

A. Estimation of state properties by random measurements

Number of occupied modes. The first useful property of the states that can be used for the classification is the number of occupied modes (d), which can be predicted by using the statistical properties of the measured single count (I), typically via the calculation of the intensity visibility, $\mathcal{V}_I := \mathrm{Var}(I)/\bar{I}^2 = 1/d$, where $\bar{I}$ is the mean of single count over many random measurements. In passing, we mention that $\sqrt{\mathcal{V}_I}$ is referred to as *speckle contrast* in literature [36,80]. The probability density function (PDF) of intensity $P_1(I/\bar{I})$ and the estimated values of d well describe all types of ground-truth states, as reported in the Supplemental Material Fig. S9 [74]. It is for instance well known that a single coherent mode will result in a contrast of 1, while the incoherent addition of d incoherent modes results in a contrast of $1/\sqrt{d}$ [36,80]. As this is only the first-order intensity correlation, it cannot be used to distinguish the set of classical states that contains coherent states and its incoherent mixtures from the complement of the classical set; it provides only information about the number of modes that the state occupies [81,82]. The well-known example includes the single-photon state and coherent state, they both occupy single mode; therefore, having $\mathcal{V}_I = 1$. In general, additional information on a state can be extracted by measuring outcomes in high-order intensity correlation functions [33,83]. In the case of random measurements, inferring the information of a state from the statistical properties of outcomes from unknown measurements is possible [68] and the generalization of the theory is still under development [84].

Purity and entanglement dimensionality. By incorporating measurements of the second-order intensity correlation function, one can obtain the purity $\mathcal{P}$ of the density matrix ρ of arbitrary monochromatic biphoton states from the first two statistical moments of intensity I and twofold coincidence C [27,68] as $\mathcal{P} = \mathrm{Tr}\rho^2 = \mathcal{V}_C - 2\mathcal{V}_I$, where $\mathcal{V}_C$ is the visibility of twofold coincidence $\mathcal{V}_C := \mathrm{Var}(C)/\overline{C}^2$, and $\overline{C}$ is the mean of twofold coincidence over many random measurements. In the case of the pure monochromatic maximally entangled biphoton state, the corresponding entanglement dimensionality ($D = d/2$) can then be estimated by $\mathcal{V}_C^{\mathrm{pure}} = 1 + 1/D$, and the PDF of twofold coincidence $P_2(C/\overline{C})$ has the analytic form of the K distribution,

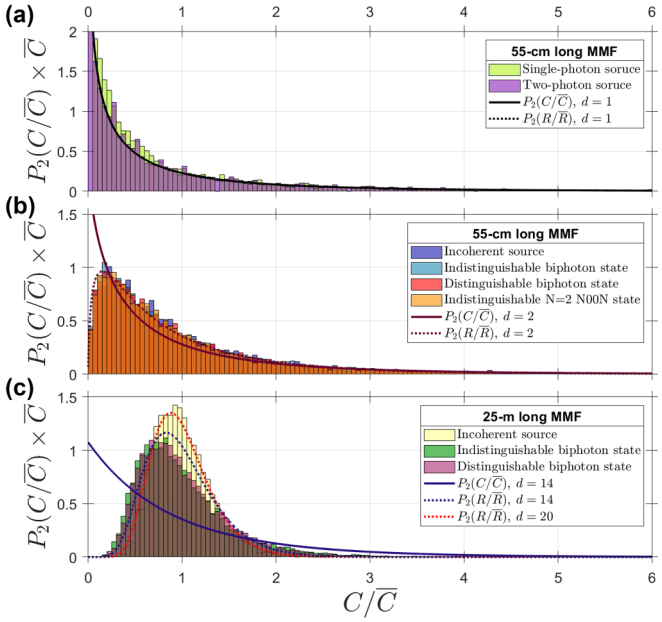

FIG. 2. Statistical distributions of twofold coincidences $P_2(C/\overline{C})$: The solid curves indicate the PDF of twofold coincidences $P_2(C/\overline{C})$ for pure d-dimensional spatially maximally entangled biphoton states, Eq. (1). The dashed curves represent the PDF of accidental coincidences $P_2(R/\overline{R})$, Eq. (2). (a) $P_2(C/\overline{C})$ for the group of single-mode states: single-photon and two-photon Fock states show the same distribution of $C/\overline{C}$ with $d = 1$. (b) $P_2(C/\overline{C})$ for the group of two-mode states propagating through the 55-cm long MMF: Indistinguishable biphoton state, $N = 2$ N00N state, distinguishable biphoton state, and incoherent source, presents no statistical difference between their distributions. (c) $P_2(C/\overline{C})$ for the group of states propagating through 25-m MMF: Indistinguishable and distinguishable biphoton states and incoherent states.

which reads

$$P_2\left(\frac{C}{\overline{C}}\right) = \frac{2d}{\Gamma(d)}\left(d\frac{C}{\overline{C}}\right)^{\frac{d-1}{2}} \mathcal{K}_{d-1}\left(2\sqrt{d\frac{C}{\overline{C}}}\right), \tag{1}$$

where Γ is the gamma function and $\mathcal{K}_{d-1}(x)$ is a modified Bessel function of the second kind.

In the experiment, we investigated the latter cases of $d = 2$ monochromatic biphoton states. The results of the measured visibilities and purity are reported in Table I and the distributions are shown in Fig. 2(b) for the indistinguishable biphoton state, $N = 2$ N00N state, and distinguishable biphoton state, which present very similar feature. Besides, they almost overlap with the distribution of the incoherent source that originates from accidental coincidence $P_2(R/\overline{R})$, which is

$$P_2\left(\frac{R}{\overline{R}}\right) = \frac{2}{\Gamma(d)^2} d^{2d}\left(\frac{R}{\overline{R}}\right)^{d-1} \mathcal{K}_0\left(2d\sqrt{\frac{R}{\overline{R}}}\right). \tag{2}$$

This thereby results in the difficulty in the classification task on these states using solely the statistics of C, albeit the ideal simulation results indicate the different distribution of the three cases at C close to 0 (as presented in Supplemental Material Fig. S1 [74]). The experimental distribution of the indistinguishable biphoton state exhibits less probability of detecting coincidence counts close to zero than that

TABLE I. Visibilities and estimated properties of ground-truth states.

State	$\mathcal{V}_I$	$\mathcal{V}_C$	$\mathcal{V}_C$*	$\mathcal{P}$	d	$\mathcal{V}_{g^{(2)}}$
Monochromatic case						
Incoherent source ($d = 2$)	0.44 ± 0.02	1.14 ± 0.06[b]	–	–	2.27 ± 0.07	0.021 ± 0.003
Biphoton state ($\delta = 0$)	0.46 ± 0.02	1.46 ± 0.09	1.38 ± 0.09	0.45 ± 0.11	2.16 ± 0.06	0.178 ± 0.009
Biphoton state ($\delta > l_c$)c	0.50 ± 0.02	1.49 ± 0.09	1.34 ± 0.09	0.35 ± 0.11	2.02 ± 0.05	0.096 ± 0.007
$N = 2$ N00N state	0.45 ± 0.02	1.43 ± 0.09	1.27 ± 0.08	0.38 ± 0.08	2.24 ± 0.01	0.127 ± 0.007
Two-photon state $\|2_V\rangle$	0.80 ± 0.04[a]	2.52 ± 0.17	2.39 ± 0.15	0.69 ± 0.22	1.23 ± 0.09	0.105 ± 0.011
Single-photon state $\|1_V\rangle$	0.81 ± 0.04[a]	2.37 ± 0.02[b]	–	–	1.23 ± 0.07	0.402 ± 0.048
Polychromatic case						
Incoherent dispersive source	0.048 ± 0.008	0.09 ± 0.01[b]	–	–	20 ± 1	0.0013 ± 0.0012
Biphoton state ($\delta = 0$)	0.068 ± 0.006	0.27 ± 0.02	0.26 ± 0.02	0.12 ± 0.02	14.7 ± 0.2	0.074 ± 0.006
Biphoton state ($\delta > l_c$)c	0.073 ± 0.006	0.26 ± 0.01	0.22 ± 0.01	0.08 ± 0.02	13.8 ± 0.3	0.049 ± 0.005

*is for indicating that the values are corrected for accidental coincidences.

[a]By subtracting estimated dark counts, $\mathcal{V}_I$ values are corrected to 0.85 ± 0.06 and 0.9 ± 0.08 for $|2_V\rangle$ and $|1_V\rangle$, respectively and resulting accordingly in the corrected d of 1.18 ± 0.09 and 1.11 ± 0.10.

[b]Contribution of accidental coincidences and $\overline{g^{(2)}} = 1$.

[c]δ is the optical delay and l_c is the two-photon coherent length.

predicted by the K distribution. We note that this effect was also present in the experimental data for high-dimensional entangled biphoton states [58]. We attribute this effect to the contribution of noise sources in each setting of random measurement, including dark counts, accidental coincidences, and finite exposure time which usually causes a broadening of the distribution. As further discussed in Supplemental Material S.6 and S.7 [74], the contribution of noise sources might be interpreted as a classical mixture of many pure biphoton states. In addition, the long tail of K distribution also results in an unreliable estimation of $\mathcal{V}_C$. Both give rise to the underestimation of the measured purity (see Table I). The use of statistical properties of the coincidences C thus has a practical limitation in the estimation of purity at low d using only the first two statistical moments.

B. On the effect of quantum interference and indistinguishability

Imperfect indistinguishability between photons affects quantum interference. One may think that the quantum interference might have signatures in the statistical distribution of twofold coincidences $P_2(C/\overline{C})$. Unfortunately, as reported above [Fig. 2(b)], this phenomenon is hardly observed in the experiment as compared to the ideal simulation [see Supplemental Material Fig. S1(a) [74]]. Here, we demonstrate nevertheless that the effect of indistinguishability can be clearly unveiled from the statistical distribution of the normalized second-order correlation function $g^{(2)}$. As presented in Fig. 3(b), in the cases of indistinguishable photons and an $N = 2$ N00N state, we observed a broader and flatter statistical distribution compared to the one associated with distinguishable photons. The key reason is that the normalized second-order correlation function $g^{(2)}$ filters out the effect of the fluctuation of intensity speckles that are present in the twofold coincidence speckles. The contribution of two-photon Hong-Ou-Mandel interference due to random projections, i.e., random varieties of HOM dips and peaks, therefore increases the variance of the distributions. The features are also evident in the simulated results (see Supplemental Material S.1D [74]) supporting our observation where we found that the distribution is uniform for the indistinguishable case as compared to the symmetric negative-log distribution $P(g^{(2)}_{\text{Dis.}}/\overline{g^{(2)}})$ for distinguishable case,

$$P\left(\frac{g^{(2)}_{\text{Dis.}}}{\overline{g^{(2)}}}\right) = -\frac{\log\left|g^{(2)}_{\text{Dis.}}/\overline{g^{(2)}} - 1\right|}{\pi\,\overline{g^{(2)}}}. \tag{3}$$

Moreover, the variance of the normalized second-order correlation for the $N = 2$ N00N state is lower than that for the indistinguishable biphoton state. This arises from the fact that the N00N state experiences dephasing effects since the state is very sensitive to phase fluctuation at the inputs of the random interferometer that modulates faster than the exposure time in each random measurement. Consequently, $g^{(2)}$ detects only the root mean square response of the fast sinusoidal oscillation arising from interference originating from the use of a N00N-state. We thus observed a $\sqrt{2}$ reduction of the variance for N00N states as compared to the case of the indistinguishable biphotons. The result is observed directly on the visibility of the normalized second-order correlation $\mathcal{V}_{g^{(2)}} := \text{Var}(g^{(2)})/\overline{g^{(2)}}^2$ where the ratio of the measured visibility between the indistinguishable biphoton state and the N00N state is $\mathcal{V}^{\text{Indis.}}_{g^{(2)}}/\mathcal{V}^{\text{N00N}}_{g^{(2)}} = 1.4 \pm 0.2 \approx \sqrt{2}$.

It is important to note that the discrepancy between the experimental distributions of $g^{(2)}$ and the prediction is due to the main contribution of dark counts and accidental coincidences. This is supported by the simulated results when the dark counts are added to single counts. As shown in Fig. 6, the simulated result shows the same tendency of the reduction in the probability of detecting $g^{(2)}$ at the high value of $g^{(2)}$ in the indistinguishable case and at around $\overline{g^{(2)}}$ in the distinguishable case as experimentally observed in Fig. 3(b). Because the distributions are still clearly distinguishable, we consider the effect minor compared to the statistical distributions of C in the previous section. Therefore, the results demonstrated the effectiveness of the statistical

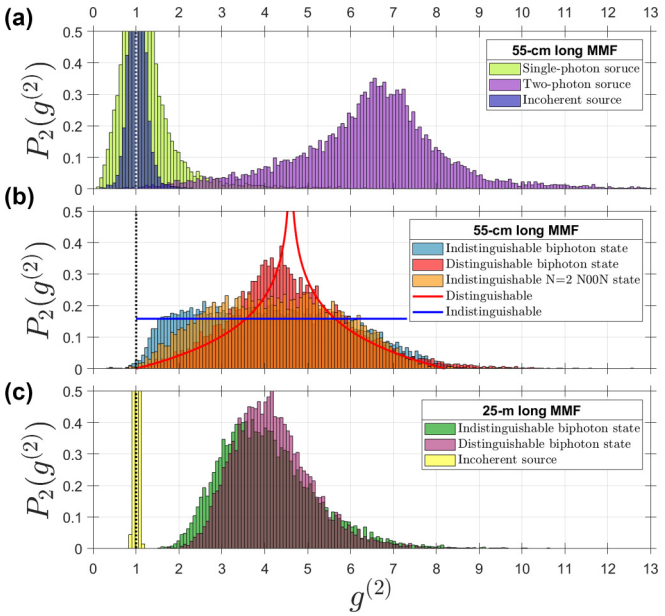

FIG. 3. Statistical distributions of experimental normalized second-order correlation $P_2(g^{(2)})$: (a) heralded single-photon state (light green), incoherent source (dark blue) and the two-photon Fock state $|2\rangle$ (magenta) in the 55-cm long MMF. The first two states have the means at the accidental coincidence (the white dashed line, $\overline{g^{(2)}} = 1$), while the two-photon Fock state shows $\overline{g^{(2)}} > 1$. (b) $P_2(g^{(2)})$ for the group of two-mode states in a 55-cm long MMF: Indistinguishable biphoton state (blue), $N = 2$ N00N state (orange), and distinguishable biphoton state (red). Their distributions are different owing to the presence of quantum interference. The histogram of indistinguishable biphotons shows the flat distribution as predicted by the probability density functions (PDF) $P_2(g^{(2)})$, represented by the blue solid line. The red curve represents the prediction for distinguishable biphotons, Eq. (3). (c) $P_2(g^{(2)})$ for the group of states evolving through the 25-m long MMF: Incoherent source (light yellow), indistinguishable (green) and distinguishable (light magenta) biphoton states. The incoherent state has the means at $\overline{g^{(2)}} = 1$, while for the biphoton states ($g^{(2)} > 1$) the width of the indistinguishable case is broader than that of the distinguishable case.

properties of the normalized second-order correlation function in distinguishing the three types of biphoton states addressed herein.

C. On the effect of dispersion on spectrally entangled biphoton states

The next question of interest is to study the statistical outcomes of unknown states propagating through the 25-m long dispersive fiber. We launched various states of light, in particular spectrally entangled biphoton states, through different spatial modes of the MMF. The modal dispersion of the MMF causes an input finite pulse to temporally spread [85,86]. In the spectral domain, this is equivalent to a narrow spectral response of the optical system, characterized by the spectral correlation bandwidth $\Delta\lambda_m$, in which a light source with bandwidth $\Delta\lambda_s$ will generate an incoherent sum of speckles over the number of temporal/spectral modes $N_\lambda = \Delta\lambda_s/\Delta\lambda_m$ [87,88]. The decrease in the outcome visibility of intensity speckles at the output of the long fiber can thus be used to estimate the number of occupied temporal/spectral modes. For spectrally entangled biphoton states, we measured the spectral incoherent modes of $\sim$7 which corresponds to the total number of occupied modes of $d \approx 14$ given the two input modes of orthogonal polarizations (see Table I for the number of occupied modes).

In Fig. 2(c), the statistical distribution of $C/\overline{C}$ for the states transmitting through the 25-m long fiber are reported. We found that the first two biphoton states show the same distribution which cannot be described by the PDF of expected accidental coincidences $P_2(R/\overline{R})$ for $d \approx 14$ predicted from the visibility of intensity. This is in contrast to the statistical distribution of the incoherent source that is well predicted by the accidental distribution of Eq. (2) using the estimated visibility of intensity of $d = 20$. In Fig. 3(c), the statistical distribution of $g^{(2)}$ for the dispersive cases shows that the statistical distribution of $g^{(2)}$ in the case of the indistinguishable biphoton state is broadened, compared to the case of the distinguishable biphoton state. This is indicated by the visibility of $g^{(2)} = 0.074 \pm 0.006$ and $g^{(2)} = 0.049 \pm 0.005$ (Table I).

It is noteworthy that the statistical signature of frequency entanglement in the dispersive case was theoretically proposed but in terms of the means of coincidence rate, $\overline{C}/\overline{R}$ [61,64], in which our experiment cannot provide the conclusive result because of the requirement of the subtle control that is sensitive to the brightness of the light sources. In terms of the statistical distributions and $\mathcal{V}_{g^{(2)}}$, the theoretical prediction is unknown, to our knowledge.

To understand the experimental results, we discuss the role of the spectral-temporal correlation of the SPDC source in a dispersive medium [61,64]. Two-photon quantum interference of spectrally entangled states is known to result in two types of dispersion cancellations: non-local and local [89–92]. At a given setting of a random interferometer, photons from biphoton pairs propagate and disperse differently through the fiber with a probability of being detected at two outputs. In the first case of non-local dispersion cancellation [91], biphoton pairs propagate to separate paths and end up detected on two separate outputs, this results in the cancellation of the dispersion of one path to another path that has the opposite sign of dispersion, therefore maintaining their twofold coincidences without the HOM interference. Whereas in the case of local dispersion cancellation [89], the HOM interference can occur, biphoton pairs that experience different dispersions have a chance to interfere and exchange their wave functions (spatial-mode mixing, i.e., a possibility that signal and idler photons have a possibility to be detected on both outputs). Two types of paths contribute to such interference: one where the two paths of a biphoton pair are directly transmitted to the detectors, and one where they exchange paths. Only relative differences in dispersion between the paths can contribute to the distinguishability. Yet, the relative differences are partially compensated owing to frequency anticorrelation that erases which-path information [90,92], resulting in the robustness of quantum interference.

We think that these are the explanation of why we observed the broadening of the statistical distribution of $g^{(2)}$ in the case of the indistinguishable biphoton state as compared to the

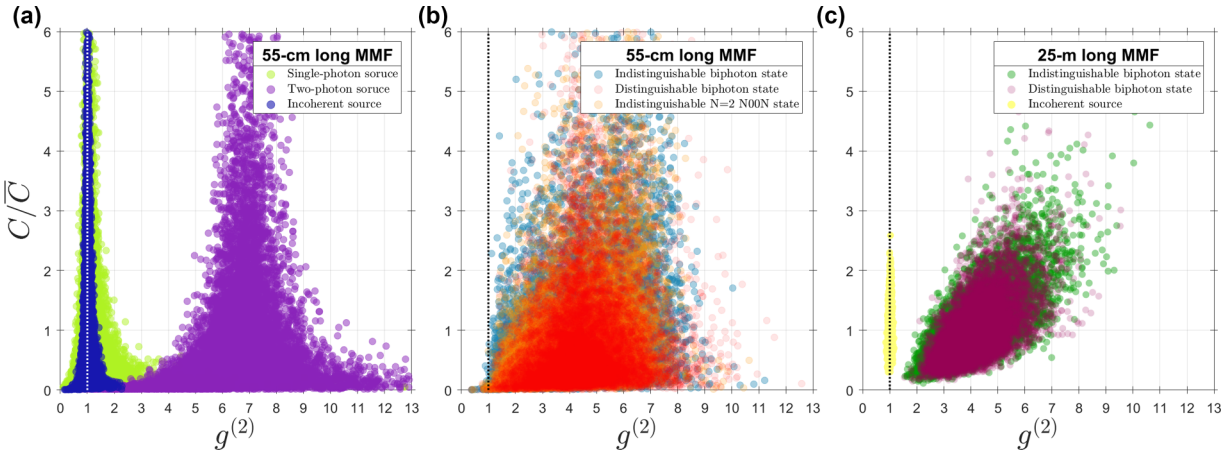

FIG. 4. Correlation of twofold coincidences $C/\overline{C}$ and normalized second-order correlation $g^{(2)}$: for a group of ground-truth state transmitting (a) and (b) through the 55-cm long multimode fiber and (c) through the 25-m long multimode fiber. Each circle on the scatter plots displays each outcome of random measurements. Note that there is the distribution of data points outside the presented area where $C/\overline{C} > 6$ and $g^{(2)} > 13$.

case of the distinguishable biphoton state in Fig. 3(c) and consider that the statistical distribution of $g^{(2)}$ is also useful for probing quantum interference in the presence of dispersion and spectral-temporal entanglement.

Lastly, we compared the measurements of the normalized second-order correlation function $g^{(2)}/\overline{g^{(2)}}$ with the analogous twofold coincidences $C/\overline{C}$ as depicted in Fig. 4. We observed that $g^{(2)}$ is clearly correlated to the two-fold coincidences C in the case of the spectrally entangled states [Fig. 4(c)], whereas this is not the case for the other states addressed here [Figs. 4(a) and 4(b)]. The positive correlation between the two indicators hence strengthens our claim in the previous section on the effect of the fluctuation in intensity speckles on the two-fold coincidence speckles since here the dispersion causes $P_1(I/\bar{I})$ to be a narrow distribution, i.e., low speckle visibility (see Supplemental Material Fig. S9(c) [74]), while the dispersion cancellations can maintain the quantum interferences, hence, resulting in a high speckle visibility in the normalized second-order correlation function $\mathcal{V}_{g^{(2)}}$.

As for the aim for classification, the distributions of $C/\overline{C}$ in Fig. 2(c) are observed to be identical for different degrees of indistinguishability and also have a feature similar to the distribution of accidental coincidences at a lower d ($d < 14$). Consequently, the state classification with information solely estimated from the statistics of twofold coincidences C, which is commonly used in literature, is not sufficient, and taking into consideration the information from the $g^{(2)}$ distribution is beneficial both for the nondispersive and dispersive cases.

D. State classification

In this section, we demonstrate the possibility of classifying states based on their statistical properties. More specifically, we are able to retrieve the number d of occupied modes, as well as the distinguishability of the input photons, through information gathered from the visibility $\mathcal{V}_I$ and normalized second-order correlation $\mathcal{V}_{g^{(2)}}$. In Fig. 5 we show how different classes of input states can be distinguished through such figures of merit. We present the visibilities estimated from 200 random measurements performed on the same experimental input state. Clearly, $\mathcal{V}_I$ and $\mathcal{V}_{g^{(2)}}$ can be used to independently probe the number of occupied modes and the distinguishability of the input states, respectively. The technique can also discriminate distinguishable from indistinguishable spectrally entangled biphoton states. The overestimation of the number of occupied modes for the single-photon and two-photon Fock states is due to the presence of dark counts, an imperfection that can be corrected (see Table I for the results after subtracting estimated dark counts). The spreading of $\mathcal{V}_{g^{(2)}}$ values for the single-photon

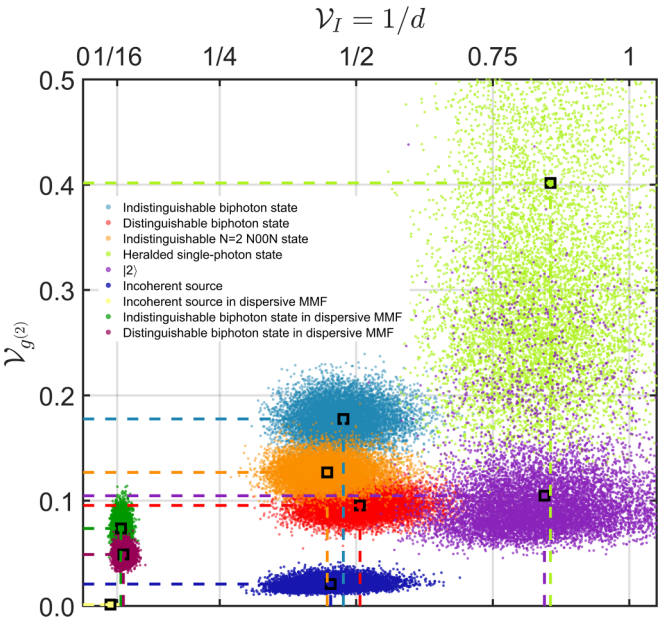

FIG. 5. Classification of input states from the intensity visibility $\mathcal{V}_I$ and the visibility of the normalized second-order correlation $\mathcal{V}_{g^{(2)}}$. The clustering patterns clearly show that the different classes of input states can be separated using only these two statistical features. In particular, it is possible to discriminate both the distinguishability and the number of occupied modes of the input states.

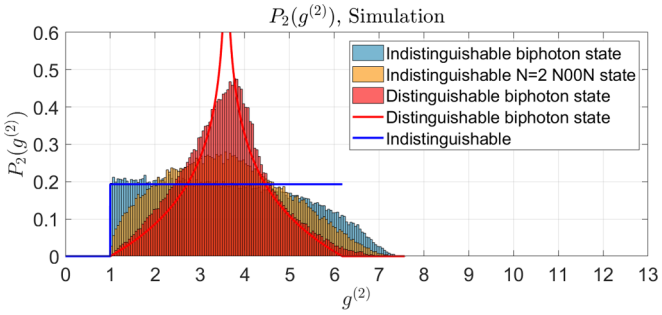

FIG. 6. Simulated statistical distribution of normalized second-order correlation in the presence of dark counts.

state results instead from accidental coincidences. Better classification performances could be achieved by incorporating the constraint $\overline{g^{(2)}} = 1$, which would help discriminate single- and two-photon Fock states.

V. CONCLUSIONS AND OUTLOOK

We have experimentally demonstrated the effectiveness of a state classifier based on the combined use of SLMs and a multimode fiber. The scheme performs state classification using the statistical properties from an ensemble of random measurements. In particular, intensity and second-order intensity correlations are used to retrieve information about the number of occupied modes, purity, and indistinguishability of the input states, without the need to perform full state tomography. The benefits and limitations of using the statistical properties of twofold coincidences C and normalized second-order correlation $g^{(2)}$ are investigated using different ground-truth states, including spectrally entangled biphoton states in the dispersive fiber. The investigation of different classes of input states, having different statistical properties, is an interesting venue for future research. In addition to the statistical properties reported here, the optical apparatus also offers the capability of implementing a reprogrammable linear optical circuit [93] and can be seamlessly incorporated with an array of coincidence detectors, hence enabling the implementation of quantum multioutcome measurements [94–96]. This allows the feasibility of performing optimal measurements, thus enabling a direct estimation of the properties of the state, e.g., purity, dimensionality, and type of entanglement. The possibility of implementing state tomography in high dimensions will be the subject of future investigations.

ACKNOWLEDGMENTS

The work is supported by European Research Council (ERC) (724473). S.G. is a member of the Institut Universitaire de France (IUF). L.I. acknowledges support from MUR and AWS under project PON Ricerca e Innovazione 2014-2020, "calcolo quantistico in dispositivi quantistici rumorosi nel regime di scala intermedia" (NISQ - Noisy, Intermediate-Scale Quantum). M.P. is supported by the European Commission through the Horizon Europe EIC Pathfinder project QuCoM (Grant Agreement No. 101046973), the Leverhulme Trust through the Research Project Grant 'Ultracold quantum thermo-machine' (UltraQuTe, Grant No. RGP-2018-266), MSCA cofunding of regional, national, and international programmes (Grant No. 754507), the Royal Society Wolfson Fellowship (RSWF/R3/183013), the UK EPSRC (Grant No. EP/T028424/1), the Department for the Economy Northern Ireland under the US-Ireland R&D Partnership Programme, the Italian National Quantum Science and Technology Institute (NQSTI) (PE0000023) - SPOKE 2 through project ASpEQCt, the National Centre for HPC, Big Data and Quantum Computing (HPC) (CN00000013) – SPOKE 10 through project HyQELM..

APPENDIX: EFFECT OF DARK COUNTS ON THE STATISTICAL DISTRIBUTION OF NORMALIZED SECOND-ORDER INTENSITY CORRELATION

The contribution of dark counts and the corresponding accidental coincidences to the statistics of the normalized second-order intensity correlation is numerically studied. The statistics of dark counts is assumed to follow a Poisson distribution. As shown in Fig. 6, we set the ratio of the average dark count to the average total count to be $1/12$ and observed the discrepancy in a similar way as found in the experiment for different input states transmitting through the 55-cm long optical fiber [Fig. 3(b)].

[1] E. P. Wigner, Random matrices in physics, SIAM Rev. **9**, 1 (1967).
[2] C. W. J. Beenakker, Random-matrix theory of quantum transport, Rev. Mod. Phys. **69**, 731 (1997).
[3] T. Guhr, A. Müller–Groeling, and H. A. Weidenmüller, Random-matrix theories in quantum physics: Common concepts, Phys. Rep. **299**, 189 (1998).
[4] B. Collins and I. Nechita, Random matrix techniques in quantum information theory, J. Math. Phys. **57**, 015215 (2016).
[5] E. J. Candès, J. Romberg, and T. Tao, Robust uncertainty principles: Exact signal reconstruction from highly incomplete frequency information, IEEE Trans. Inf. Theory **52**, 489 (2006).
[6] A. Rahimi and B. Recht, Random features for large-scale kernel machines, in *Proceedings of the 20th International Conference on Neural Information Processing Systems (NIPS'07)* (Curran Associates Inc., Red Hook, NY, USA, 2007), pp. 1177–1184.
[7] M. W. Mahoney, Randomized algorithms for matrices and data, FNT in Machine Learning in Machine Learning **3**, 123 (2010).
[8] J. Schlienz and G. Mahler, Description of entanglement, Phys. Rev. A **52**, 4396 (1995).
[9] W. Laskowski, D. Richart, C. Schwemmer, T. Paterek, and H. Weinfurter, Experimental Schmidt decomposition and state independent entanglement detection, Phys. Rev. Lett. **108**, 240501 (2012).
[10] M. C. Tran, B. Dakić, F. Arnault, W. Laskowski, and T. Paterek, Quantum entanglement from random measurements, Phys. Rev. A **92**, 050301 (2015).

[11] T. Brydges, A. Elben, P. Jurcevic, B. Vermersch, C. Maier, B. P. Lanyon, P. Zoller, R. Blatt, and C. F. Roos, Probing Rényi entanglement entropy via randomized measurements, Science **364**, 260 (2019).

[12] A. Ketterer, N. Wyderka, and O. Gühne, Entanglement characterization using quantum designs, Quantum **4**, 325 (2020).

[13] L. Knips, A moment for random measurements, Quantum Views **4**, 47 (2020).

[14] S. Liu, Q. He, M. Huber, O. Gühne, and G. Vitagliano, Characterizing entanglement dimensionality from randomized measurements, PRX Quantum **4**, 020324 (2023).

[15] N. Wyderka, A. Ketterer, S. Imai, J. L. Bönsel, D. E. Jones, B. T. Kirby, X.-D. Yu, and O. Gühne, Complete characterization of quantum correlations by randomized measurements, Phys. Rev. Lett. **131**, 090201 (2023).

[16] J. Emerson, R. Alicki, and K. Życzkowski, Scalable noise estimation with random unitary operators, J. Opt. B: Quantum Semiclassical Opt. **7**, S347 (2005).

[17] A. Elben, B. Vermersch, R. van Bijnen, C. Kokail, T. Brydges, C. Maier, M. K. Joshi, R. Blatt, C. F. Roos, and P. Zoller, Cross-platform verification of intermediate scale quantum devices, Phys. Rev. Lett. **124**, 010504 (2020).

[18] J. Eisert, D. Hangleiter, N. Walk, I. Roth, D. Markham, R. Parekh, U. Chabaud, and E. Kashefi, Quantum certification and benchmarking, Nat. Rev. Phys. **2**, 382 (2020).

[19] J. Helsen, I. Roth, E. Onorati, A. H. Werner, and J. Eisert, General framework for randomized benchmarking, PRX Quantum **3**, 020357 (2022).

[20] D. Gross, Y.-K. K. Liu, S. T. Flammia, S. Becker, and J. Eisert, Quantum state tomography via compressed sensing, Phys. Rev. Lett. **105**, 150401 (2010).

[21] D. Oren, M. Mutzafi, Y. C. Eldar, and M. Segev, Quantum state tomography with a single measurement setup, Optica **4**, 993 (2017).

[22] J. G. Titchener, M. Gr, A. S. Solntsev, A. Szameit, A. A. Sukhorukov, M. Gräfe, R. Heilmann, A. S. Solntsev, A. Szameit, and A. A. Sukhorukov, Scalable on-chip quantum state tomography, npj Quantum Inf. **4**, 19 (2018).

[23] K. Wang, J. G. Titchener, S. S. Kruk, L. Xu, H.-P. Chung, M. Parry, I. I. Kravchenko, Y.-H. Chen, A. S. Solntsev, Y. S. Kivshar, D. N. Neshev, and A. A. Sukhorukov, Quantum metasurface for multiphoton interference and state reconstruction, Science **361**, 1104 (2018).

[24] L. De Santis, G. Coppola, C. Antón, N. Somaschi, C. Gómez, A. Lemaître, I. Sagnes, L. Lanco, J. C. Loredo, O. Krebs, and P. Senellart, Overcomplete quantum tomography of a path-entangled two-photon state, Phys. Rev. A **99**, 022312 (2019).

[25] L. Banchi, W. S. Kolthammer, and M. S. Kim, Multiphoton tomography with linear optics and photon counting, Phys. Rev. Lett. **121**, 250402 (2018).

[26] L. Innocenti, S. Lorenzo, I. Palmisano, F. Albarelli, A. Ferraro, M. Paternostro, and G. M. Palma, Shadow tomography on general measurement frames, PRX Quantum **4**, 040328 (2023).

[27] S. J. van Enk and C. W. J. Beenakker, Measuring $\mathrm{Tr}\rho^n$ on single copies of ρ using random measurements, Phys. Rev. Lett. **108**, 110503 (2012).

[28] A. Dimić and B. Dakić, Single-copy entanglement detection, npj Quantum Inf. **4**, 11 (2018).

[29] V. Saggio, A. Dimić, C. Greganti, L. A. Rozema, P. Walther, and B. Dakić, Experimental few-copy multipartite entanglement detection, Nat. Phys. **15**, 935 (2019).

[30] H.-Y. Y. Huang, R. Kueng, and J. Preskill, Predicting many properties of a quantum system from very few measurements, Nat. Phys. **16**, 1050 (2020).

[31] L. Innocenti, S. Lorenzo, I. Palmisano, A. Ferraro, M. Paternostro, and G. M. Palma, Potential and limitations of quantum extreme learning machines, Commun. Phys. **6**, 118 (2023).

[32] A. Elben, S. T. Flammia, H.-Y. Huang, R. Kueng, J. Preskill, B. Vermersch, and P. Zoller, The randomized measurement toolbox, Nat. Rev. Phys. **5**, 9 (2023).

[33] P. Cieśliński, S. Imai, J. Dziewior, O. Gühne, L. Knips, W. Laskowski, J. Meinecke, T. Paterek, and T. Vértesi, Analysing quantum systems with randomised measurements, Phys. Rep. **1095**, 1 (2024).

[34] C. W. J. Beenakker, Classical and quantum optics, in *The Oxford Handbook of Random Matrix Theory* (Oxford University Press, Oxford, 2015).

[35] S. Rotter and S. Gigan, Light fields in complex media: Mesoscopic scattering meets wave control, Rev. Mod. Phys. **89**, 015005 (2017).

[36] J. W. Goodman, *Speckle Phenomena in Optics: Theory and Applications* (Roberts and Company Publishers, Boston, 2005), pp. 1–228.

[37] R. J. Glauber, The quantum theory of optical coherence, Phys. Rev. **130**, 2529 (1963).

[38] B. E. A. Saleh, A. F. Abouraddy, A. V. Sergienko, and M. C. Teich, Duality between partial coherence and partial entanglement, Phys. Rev. A **62**, 043816 (2000).

[39] O. Lib and Y. Bromberg, Quantum light in complex media and its applications, Nat. Phys. **18**, 986 (2022).

[40] A. Aiello and J. P. Woerdman, Intrinsic entanglement degradation by multimode detection, Phys. Rev. A **70**, 023808 (2004).

[41] J. L. Van Velsen and C. W. J. Beenakker, Transition from pure-state to mixed-state entanglement by random scattering, Phys. Rev. A **70**, 032325 (2004).

[42] G. Puentes, A. Aiello, D. Voigt, and J. P. Woerdman, Entangled mixed-state generation by twin-photon scattering, Phys. Rev. A **75**, 032319 (2007).

[43] M. Candé, A. Goetschy, and S. E. Skipetrov, Transmission of quantum entanglement through a random medium, Europhys. Lett. **107**, 54004 (2014).

[44] G. Sorelli, V. N. Shatokhin, F. S. Roux, and A. Buchleitner, Entanglement of truncated quantum states, Quantum Sci. Technol. **5**, 035012 (2020).

[45] M. Patra and C. W. J. Beenakker, Propagation of squeezed radiation through amplifying or absorbing random media, Phys. Rev. A **61**, 063805 (2000).

[46] P. Lodahl and A. Lagendijk, Transport of quantum noise through random media, Phys. Rev. Lett. **94**, 153905 (2005).

[47] P. Lodahl, Quantum noise frequency correlations of multiply scattered light, Opt. Lett. **31**, 110 (2006).

[48] P. Lodahl, Quantum correlations induced by multiple scattering of quadrature squeezed light, Opt. Express **14**, 6919 (2006).

[49] S. E. Skipetrov, Quantum theory of dynamic multiple light scattering in fluctuating disordered media, Phys. Rev. A **75**, 053808 (2007).

[50] Y. Bromberg, Y. Lahini, R. Morandotti, and Y. Silberberg, Quantum and classical correlations in waveguide lattices, Phys. Rev. Lett. **102**, 253904 (2009).

[51] Y. Lahini, Y. Bromberg, D. N. Christodoulides, and Y. Silberberg, Quantum correlations in two-particle Anderson localization, Phys. Rev. Lett. **105**, 163905 (2010).

[52] J. Carolan, J. D. A. Meinecke, P. J. Shadbolt, N. J. Russell, N. Ismail, K. Wörhoff, T. Rudolph, M. G. Thompson, J. L. O'Brien, J. C. F. Matthews, and A. Laing, On the experimental verification of quantum complexity in linear optics, Nat. Photon. **8**, 621 (2014).

[53] H. E. Kondakci, A. Szameit, A. F. Abouraddy, D. N. Christodoulides, and B. E. A. Saleh, Sub-thermal to super-thermal light statistics from a disordered lattice via deterministic control of excitation symmetry, Optica **3**, 477 (2016).

[54] P. Lodahl, A. P. Mosk, and A. Lagendijk, Spatial quantum correlations in multiple scattered light, Phys. Rev. Lett. **95**, 173901 (2005).

[55] S. Smolka, A. Huck, U. L. Andersen, A. Lagendijk, and P. Lodahl, Observation of spatial quantum correlations induced by multiple scattering of nonclassical light, Phys. Rev. Lett. **102**, 193901 (2009).

[56] W. H. Peeters, J. J. D. Moerman, and M. P. van Exter, Observation of two-photon speckle patterns, Phys. Rev. Lett. **104**, 173601 (2010).

[57] M. P. Van Exter, J. Woudenberg, H. D. L. Pires, and W. H. Peeters, Bosonic, fermionic, and anyonic symmetry in two-photon random scattering, Phys. Rev. A **85**, 033823 (2012).

[58] H. D. L. Pires, J. Woudenberg, and M. P. Van Exter, Statistical properties of two-photon speckles, Phys. Rev. A **85**, 033807 (2012).

[59] S. Smolka, O. L. Muskens, A. Lagendijk, and P. Lodahl, Angle-resolved photon-coincidence measurements in a multiple-scattering medium, Phys. Rev. A **83**, 043819 (2011).

[60] J. R. Ott, N. A. Mortensen, and P. Lodahl, Quantum interference and entanglement induced by multiple scattering of light, Phys. Rev. Lett. **105**, 090501 (2010).

[61] M. Candé and S. E. Skipetrov, Quantum versus classical effects in two-photon speckle patterns, Phys. Rev. A **87**, 013846 (2013).

[62] I. Starshynov, J. Bertolotti, and J. Anders, Quantum correlation of light scattered by disordered media, Opt. Express **24**, 4662 (2016).

[63] L. Rigovacca, C. Di Franco, B. J. Metcalf, I. A. Walmsley, and M. S. Kim, Nonclassicality criteria in multiport interferometry, Phys. Rev. Lett. **117**, 213602 (2016).

[64] N. Cherroret and A. Buchleitner, Entanglement and Thouless times from coincidence measurements across disordered media, Phys. Rev. A **83**, 033827 (2011).

[65] M. Walschaers, J. Kuipers, J. D. Urbina, K. Mayer, M. C. Tichy, K. Richter, and A. Buchleitner, Statistical benchmark for Boson sampling, New J. Phys. **18**, 032001 (2016).

[66] D. Li, Y. Yao, and M. Li, Statistical distribution of quantum correlation induced by multiple scattering in the disordered medium, Opt. Commun. **446**, 106 (2019).

[67] D. S. Phillips, M. Walschaers, J. J. Renema, I. A. Walmsley, N. Treps, and J. Sperling, Benchmarking of Gaussian Boson sampling using two-point correlators, Phys. Rev. A **99**, 023836 (2019).

[68] C. W. J. Beenakker, J. W. F. Venderbos, and M. P. Van Exter, Two-photon speckle as a probe of multi-dimensional entanglement, Phys. Rev. Lett. **102**, 193601 (2009).

[69] M. Walschaers, J. Kuipers, and A. Buchleitner, From many-particle interference to correlation spectroscopy, Phys. Rev. A **94**, 020104 (2016).

[70] T. Giordani, F. Flamini, M. Pompili, N. Viggianiello, N. Spagnolo, A. Crespi, R. Osellame, N. Wiebe, M. Walschaers, A. Buchleitner, and F. Sciarrino, Experimental statistical signature of many-body quantum interference, Nat. Photon. **12**, 173 (2018).

[71] J. Qin, D. Wu, X. Ding, Y. Hu, P. Hu, X.-yan Yang, W.-jun Zhang, H. Li, Y. Li, X. Jiang, L. Gan, G. Yang, L. You, Z. Wang, L. Li, N.-L. Liu, C.-Y. Lu, J.-W. Pan, H.-sen Zhong, H. Wang *et al.*, Quantum computational advantage using photons, Science **370**, 1460 (2020).

[72] K. Zyczkowski and H.-J. Sommers, Truncations of random unitary matrices, J. Phys. A **33**, 2045 (2000).

[73] S. Aaronson and A. Arkhipov, The computational complexity of linear optics, in *Proceedings of the 43rd Annual ACM Symposium on Theory of Computing - STOC '11*, 0844626 (ACM Press, New York, 2011), p. 333.

[74] See Supplemental Material at http://link.aps.org/supplemental/10.1103/PhysRevResearch.7.023222 for S.1 theoretical frameworks and simulation, S.2 experimental setup, S.3 statistical analysis of random measurements, S.4 experimental parameters and status of ground-truth light sources, S.5 SPDC source, S.6 underestimation of the purity, S.7 contribution of noises on the statistical distributions, and S.8 statistical distribution of intensity.

[75] D. Ljunggren and M. Tengner, Optimal focusing for maximal collection of entangled narrow-band photon pairs into single-mode fibers, Phys. Rev. A **72**, 062301 (2005).

[76] V. Srivastav, N. H. Valencia, S. Leedumrongwatthanakun, W. McCutcheon, and M. Malik, Characterizing and tailoring spatial correlations in multimode parametric down-conversion, Phys. Rev. Appl. **18**, 054006 (2022).

[77] C. K. Hong, Z. Y. Ou, and L. Mandel, Measurement of subpicosecond time intervals between two photons by interference, Phys. Rev. Lett. **59**, 2044 (1987).

[78] H. Lee, P. Kok, and J. P. Dowling, A quantum rosetta stone for interferometry, J. Mod. Opt. **49**, 2325 (2002).

[79] A. I. Lvovsky, H. Hansen, T. Aichele, O. Benson, J. Mlynek, and S. Schiller, Quantum state reconstruction of the single-photon fock state, Phys. Rev. Lett. **87**, 050402 (2001).

[80] J. W. Goodman, Some fundamental properties of speckle, J. Opt. Soc. Am. **66**, 1145 (1976).

[81] R. J. Glauber, Coherent and incoherent states of the radiation field, Phys. Rev. **131**, 2766 (1963).

[82] C. Fabre and N. Treps, Modes and states in quantum optics, Rev. Mod. Phys. **92**, 035005 (2020).

[83] K. Laiho, T. Dirmeier, M. Schmidt, S. Reitzenstein, and C. Marquardt, Measuring higher-order photon correlations of faint quantum light: A short review, Phys. Lett. A **435**, 128059 (2022).

[84] E. Brunner, A. Buchleitner, and G. Dufour, Many-body coherence and entanglement probed by randomized correlation measurements, Phys. Rev. Res. **4**, 043101 (2022).

[85] X. Shen, J. M. Kahn, and M. A. Horowitz, Compensation for multimode fiber dispersion by adaptive optics, Opt. Lett. **30**, 2985 (2005).

[86] J. Carpenter, B. J. Eggleton, and J. Schröder, Observation of Eisenbud-Wigner-Smith states as principal modes in multimode fibre, Nat. Photon. **9**, 751 (2015).

[87] D. Andreoli, G. Volpe, S. Popoff, O. Katz, S. Grésillon, and S. Gigan, Deterministic control of broadband light through a multiply scattering medium via the multispectral transmission matrix, Sci. Rep. **5**, 10347 (2015).

[88] M. Mounaix, D. Andreoli, H. Defienne, G. Volpe, O. Katz, S. Grésillon, and S. Gigan, Spatiotemporal coherent control of light through a multiple scattering medium with the multispectral transmission matrix, Phys. Rev. Lett. **116**, 253901 (2016).

[89] A. M. Steinberg, P. G. Kwiat, and R. Y. Chiao, Dispersion cancellation in a measurement of the single-photon propagation velocity in glass, Phys. Rev. Lett. **68**, 2421 (1992).

[90] A. M. Steinberg, P. G. Kwiat, and R. Y. Chiao, Dispersion cancellation and high-resolution time measurements in a fourth-order optical interferometer, Phys. Rev. A **45**, 6659 (1992).

[91] J. D. Franson, Nonlocal cancellation of dispersion, Phys. Rev. A **45**, 3126 (1992).

[92] J. D. Franson, Nonclassical nature of dispersion cancellation and nonlocal interferometry, Phys. Rev. A **80**, 032119 (2009).

[93] S. Leedumrongwatthanakun, L. Innocenti, H. Defienne, T. Juffmann, A. Ferraro, M. Paternostro, and S. Gigan, Programmable linear quantum networks with a multimode fibre, Nat. Photon. **14**, 139 (2020).

[94] C. Bruschini, H. Homulle, I. M. Antolovic, S. Burri, and E. Charbon, Single-photon avalanche diode imagers in biophotonics: Review and outlook, Light: Sci. Appl. **8**, 87 (2019).

[95] S. Goel, S. Leedumrongwatthanakun, N. H. Valencia, W. McCutcheon, A. Tavakoli, C. Conti, P. W. H. Pinkse, and M. Malik, Inverse design of high-dimensional quantum optical circuits in a complex medium, Nat. Phys. **20**, 232 (2024).

[96] A. Makowski, M. Dąbrowski, I. M. Antolovic, C. Bruschini, H. Defienne, E. Charbon, R. Lapkiewicz, and S. Gigan, Large reconfigurable quantum circuits with SPAD arrays and multimode fibers, Optica **11**, 340 (2024).